Kidney pathological changes alter cell clustering features in single-cell RNA sequencing

Lijun Ma[1], Mariana Murea[1], Young A Choi[1], Ashok K. Hemal[2], Alexei V. Mikhailov[3], James A. Snipes[1], Jeff W. Chou[4], Wei Cui[4], Lance D. Miller[4], Gregory A. Hawkins[4,5], Nicholette D. Palmer[5], Carl D. Langefeld[6], Barry I. Freedman[1]

[1]Department of Internal Medicine, Section on Nephrology

[2]Department of Urology

[3]Department of Pathology

[4]Department of Cancer Biology

[5]Department of Biochemistry

[6]Department of Biostatistics and Data Sciences

Wake Forest School of Medicine

Winston Salem, NC 27157

Corresponding author:

Lijun Ma, MD, PhD

lima@wakehealth.edu

Abstract

The kidney is composed of multiple cell types, each with specific physiological functions. Single-cell RNA sequencing (scRNA-Seq) is useful for classifying cell-specific gene expression profiles in kidney tissue. Because viable cells are critical in scRNA-Seq analyses, we report an optimized cell dissociation process and the necessity for histological screening of human kidney sections prior to performing scRNA-Seq. We show that glomerular injury can result in loss of select cell types during the cell clustering process. Subsequent fluorescence microscopy confirmed reductions in cell-specific markers among the injured cells seen on kidney sections and these changes need to be considered when interpreting results of scRNA-Seq.

Introduction

Due to the heterogeneity of cell types in the kidney, researchers have proposed and performed microdissection-based expression quantitative trait loci (eQTL) analyses on human kidney cell fractions[1]. More recently, single-cell RNA sequencing (scRNA-Seq) has been recognized as a cutting-edge technique in the classification of cell-specific gene expression profiles, particularly important in determining cell-specific mechanisms in kidney disease. In order to perform cell-specific kidney tissue eQTL analysis or differential gene expression studies, clinical biopsies from human kidneys are the major source of samples for scRNA-Seq. It is crucial to maintain cell viability for scRNA-Seq; however, many cells may not survive tissue processing. This is true for kidney cells in patients with renal disease, especially important for patients with more advanced changes such as focal segmental glomerulosclerosis (FSGS) and prior to transplant of kidneys with prolonged cold ischemia. In similar fashion, pre-transplant kidney histology often impacts the decision to discard deceased donor kidneys as injury may

negatively affect transplant outcomes. Hence, approximately 20% of all deceased donor kidneys are discarded[2]; the discard rate rises to 24% in African American deceased donor kidneys in the *APOL1* Long-term Kidney Transplant Outcomes (APOLLO) Study (personal communication, Freedman BI). These concerns support the need to assess kidney histology on biopsy samples obtained from nephrectomies or clinical biopsies prior to analyzing the samples with scRNA-Seq, because viable cell populations are critical for scRNA Seq.

Methods

Collection of nephrectomy specimens

Four patients who underwent nephrectomy for renal cell carcinoma between 8/23-9/26/2013 were randomly selected from our repository to verify the quality of enriched glomerular cells that had been stored in liquid nitrogen (LN2) for extended periods. Patient age, sex, diabetes, and post-surgical complications were recorded. Preoperative serum creatinine and estimated glomerular filtration rate (eGFR) were obtained. Only patients with a preoperative CKD EPI eGFR >60 ml/min/1.73 m^2 were enrolled. Basic demographic data are shown in Supplementary Table S1. The Institutional Review Board at the Wake Forest School of Medicine approved the protocol and all patients provided written informed consent.

Specimen processing and sc-RNA-Seq.

After removal of the kidney, cortical tissue was immediately dissected in the operating room to obtain non-diseased tissue. Macroscopically healthy tissue was immediately washed with sterile Hank's balanced salt solution (HBSS; Lonza, Walkersville, MD), and (1) placed in a biopsy cassette (Fisher HealthCare, Houston, TX), and immersed in 4% paraformaldehyde for

preparation of paraffin-embedded kidney tissue blocks, (2) rapidly frozen in optimal cutting temperature gel (Sukaru FineTek Inc., Torrance, CA) to create cryosections for immunofluorescence studies, and (3) kept in Dulbecco's Modified Eagle Medium (DMEM; Invitrogen, Grand Island, NY) media with 10% fetal bovine serum (FBS) on a surface of ice or 4°C refrigeration for up to 36 hours (mimicking the maximum time frame for transplantation after donor kidney recovery) until the next step in glomerular enrichment.

After removal from DMEM, kidney tissues were washed on ice in HBSS (Lonza, Walkersville, MD). Cortical tissue was cut into 1 mm^3 fragments and digested with 2 mg/ml collagenase type II at 37° C in DMEM (Invitrogen, Grand Island, NY) for 40 min. The suspension was passed through a 250 μm sieve (Sigma, St. Louis, MO) with minimum pressure. The flow through was subsequently passed through a 100 μm cell strainer (BD BioSciences). Glomeruli were collected on the surface of the strainer. After three washes with HBSS, glomeruli were suspended in 1 ml DMEM containing 0.5% BSA in a 1.5 ml centrifuge tube, and incubated at room temperature for 30 minutes with gentle agitation. Enrichment of glomeruli were assessed via light microscopy using a drop of the suspension (Supplementary Figure S1). The glomerular suspension was digested with 0.5 mg/ml of collagenase (Invitrogen), 0.5 mg/ml dispase II (ZenBio, Research Triangle Park, NC), and 0.075% trypsin in DMEM at 37° C for 25 minutes with gentle rotation. Detached cells were treated with DMEM containing 10% FBS to neutralize proteases and centrifuged at 300 x g for 3 minutes. The cell pellet was re-suspended and cultured in Endothelial Cell Growth Media (EGM2)-MV (Lonza, Walkersville, MD) for 2 days before trypsinization. Cells were viably frozen in DMEM with 20% heat-inactivated FBS and 10% Hybri-Max Dimethyl Sulfoxide (DMSO; Sigma-Aldrich): by cooling in isopropanol at −1°C per minute at −80°C overnight, and subsequently stored under LN2 vapor. In preparation for

scRNA-seq, cells were thawed and washed according to the protocol for human peripheral blood mononuclear cells (PBMCs; 10× Genomics). All scRNA-seq procedures were performed by the Cancer Genomics Shared Resource (CGSR) of Wake Forest School of Medicine. Viable cells (mean 85.35% ± 2.3%, n = 4) in suspensions averaging 1205 ± 130 cell/µl were loaded into wells of a 10× Chromium single cell capture chip targeting a cell recovery rate of 2000 - 4000 cells. Single-cell gel beads in emulsion (GEMs) were created on a Chromium Single Cell Controller and scRNA-seq libraries were prepared using the Chromium Single Cell 3' Library and Gel Bead kit according to the manufacturer's protocol (10× Genomics). Sequencing libraries were loaded at 1.3 PM on an Illumina NextSeq500 with High Output 150 cycle kit (Illumina) for paired-end sequencing using the following read length: 26 bp Read1, 8 bp i7 Index, 0 bp i5 Index, and 98 bp Read2). Technical procedures are highlighted in Supplementary Figure S1.

Histological examination and immunofluorescence imaging

Formalin-fixed paraffin-embed (FFPE) kidney tissue blocks were sliced into 3 µm thickness sections of for staining with hematoxylin and eosin (HE); digital images were obtained on a Zeiss Axioplan 2 microscope. Immunofluorescence of podocin (Sigma, St Louis, MO), CD31 (BD Biosciences), and VCAM1 (Invitrogen) was performed on kidney cryo-sections using established protocols[3] from patients who underwent HE staining of FFPE sections for histologic examination. Information for primary antibodies is summarized in Supplementary Table S2. Secondary antibodies (donkey anti-goat Alexa Fluor 594, and goat anti-mouse Alexa Fluor 488, Jackson ImmunoResearch Laboratories) were used to display fluorescent signals (1:100 dilution).Immunofluorescence imaging was performed on an Olympus IX71 fluorescence microscope (Olympus Scientific Solutions Americas Corp., Waltham, Massachusetts).

Processing of scRNA-Seq data

Cell Ranger Single Cell Software Suite v.2.0.1 was used to perform sample de-multiplexing, alignment, filtering, and UMI (i.e. universal molecular identifier) counting (https://support.10xgenomics.com/single-cell-gene expression/software/pipelines/latest/what-is-cell-ranger). The data for each respective subpopulation were aggregated for direct comparison of single cell transcriptomes. A total of 11,259 single cells from the 4 samples were captured, with the number of cells recovered per channel ranging from 2486 to 3546. The mean reads per cell varied from 63,761 and 88,599 with median Unique Molecular Indexes of 3,429 to 5,257 per cell. For T-distributed Stochastic Neighbor Embedding (tSNE) projection and clustering analysis, we used the first 30 principal components, determined using the standard deviations of the principal components visualized by Cell Ranger. The feature plot function was used to highlight expression. A false discovery rate (FDR) p-value and fold change were used to estimate the differential expression of transcripts grouped in the specific cluster vs. remaining clusters.

Results

Histologic findings on HE stained FFPE sections

Figure 1 displays normal glomerular and tubular structures in patients A, B and D. Patient A had long-standing diabetes. The biopsy from Patient C (Figure 1) showed dilated afferent and efferent arterioles as well as the capillaries of the glomerular tuft and the peritubular capillaries, containing crowded red blood cells. There was diffuse mild to moderate acute tubular injury. As a possible etiology, we considered venous outflow obstruction due to compression of the renal vein(s) by the tumor, venous thrombosis due to paraneoplastic effects, systemic disease, and

thrombotic microangiopathy. Although no diagnostic features of thrombotic microangiopathy were seen, the patient subsequently developed deep vein thrombosis after nephrectomy.

Kidney cell types, grouped by scRNA Seq features

Figure 2a displays the major kidney cell types in the four study participants, grouped by cell-specific markers. The top 5 transcripts for each cell cluster are summarized in Supplementary Table S3. Podocytes were classified by a number of known markers, with *NPHS2* (podocin) as the top marker with FDR p-value=$6x10^{-265}$ (log_2[fold-change]=9.39). Glomerular endothelial cells were well clustered by known markers with *PECAM1* (CD31) ranking highest for its FDR p-value=$9x10^{-151}$ (log_2[fold-change]=9.76). Another cluster of endothelial cells were detected, featured by top marker *VCAM1* with FDR p-value=$6.0x10^{-38}$ (log_2[fold-change]=2.23). *VACAM1* encodes a cell surface sialoglycoprotein expressed by cytokine-activated endothelial cells. Mesangial cells were characterized by a series of markers, where *HHIP* (hedgehog interacting protein) was at the top with an FDR p-value=$6x10^{-114}$ (log_2[fold-change]=3.35). *HHIP* is a novel intracellular mesangial cell marker, which interacts with TGFβ1 and known to play a role in mesangial expansion with diabetic kidney disease[4].

A key observation from review of individual feature plots was that podocin-positive cells and CD31-positive glomerular endothelial cells were absent from patient C (Figure 2b). We speculate that glomerular endothelial cell injury as a result of glomerular circulatory changes in this individual led to podocyte dysfunction. Patient C had well clustered proximal tubule and distal tubule cells as shown in the other three patients in the aggregated feature plot (Figure 2 a,b) based on their corresponding cell markers, *i.e.*, *ANPEP* (Aminopeptidase N, CD13) as top proximal tubule marker[5] (FDR p-value=$5x10^{-123}$, log_2[fold-change]=3.44) and *RAB25* as top

distal tubule and collecting duct marker[6] (FDR p-value=$2x10^{-299}$, $\log_2$[fold-change]=6.31). For the aggregated feature plot of all four patients, the macrophage cluster was readily detected by top markers *C1QA*, *C1QB*, and *C1QC* with FDR p-values=$5x10^{-157}$, $3x10^{-154}$, and $2x10^{-139}$, respectively; $\log_2$[fold-change] 11.80 for all. The final group of cells were classified as "undetermined" (Figure 2a, Supplementary Table 3), featured by a group of overexpressed mitochondrion-encoded genes (Supplementary Figure S2). The lactate dehydrogenase *LDHA* expression level in these cells was lower than among other cell clusters, indicating metabolic inactivity (Supplementary Figure S3). It is possible some of these cells were in the process of dying (85% of cells were viable in this cell pool) or they could be silent glomerular progenitor cells that would later develop into mature glomerular cells[7] or podocytes[8]. Hence, we did not remove these cells and marked them as "undetermined" to avoid the potential for bias.

Verification of impacted cell clusters by immunofluorescence on kidney cryo-sections

To assess the discrepancies of cell grouping patterns across the four kidney biopsy samples in the scRNA-Seq feature plot (missing podocyte and glomerular endothelial cell clusters in patient C), we examined the immunofluorescence staining of podocin, CD31 and VCAM1 using cryo-sections from the same four patients who underwent FFPE-based HE staining and scRNA-Seq of glomerular cell-enriched cell suspension. Podocin and CD31 signals were markedly lower in patient C than in the other patients; however, they displayed typical glomerular podocyte and endothelial cell patterns, respectively, as seen in patients A, B, and D (Supplementary Figures S4 & S5). Across all four patients, VCAM1 appeared to display Bowman's capsule and peritubular endothelial cell patterns (Supplementary Figure S6),

consistent with prior reports that VCAM-1 is present on parietal epithelial cells lining Bowman's capsule[9] and peritubular endothelial cells[10].

Discussion

Kidney specimens comprising enriched glomerular cells, cryo-tissue blocks, and FFPE tissue blocks collected nearly eight years prior were selected to assess the effect of LN2 preservation time on scRNA-Seq cell cluster patterns. The importance of scRNA-Seq in human kidney tissue is critical as different kidney cells possess unique functions. Glomerular cells occupy a small fraction of the total kidney cell volume. As such, scRNA-Seq in whole kidney compartments (cortex or interstitium) or cell collections not enriched for glomerular cells may result in the loss of podocytes and other glomerular cells during clustering due to dilution from massive volumes of tubule cells[11]. The technique of microdissection requires highly trained personnel to complete the process in a short time; however, cell dissociation is still required[1]. Fluorescence-activated cell sorting (FACS)[12] before scRNA-Seq is feasible for small samples. For scRNA-Seq studies involving more than 50 individuals, FACS would be time-consuming, expensive, and difficult to complete in a narrow time window resulting in potential batch effects.

Previous reports of scRNA-Seq in glomerular-enriched cells were performed shortly after FACS sorting, without allowing time for cell recovery. In contrast, we provided cells two additional days in recovery media which led to cell survival after nearly 8 years of storage in LN2. The modified cell dissociation method applied in this study avoided FACS[12], yet obtained similar cell clusters after scRNA-Seq as those implementing FACS. Although proximal and distal tubule cell numbers were higher in the clustering feature plot, this did not affect the quality of glomerular cell clustering.

One patient (Patient C) in our study showed markedly dilated arterioles and capillaries packed with red blood cells, and acute tubular injury. Abnormal blood flow in the glomeruli has been shown to induce endothelial injury and damage podocytes[13]. To assess the viability of all glomerulus-enriched cells and to assess the validity of cells in the scRNA-Seq analysis, we performed cell dissociation of enriched glomerular cell mixtures from all four patients. The overall scRNA-Seq cell clustering plot revealed the major glomerular cell types with reasonable mixtures of proximal tubule and distal tubule cells. However, podocin-positive and CD31-positive cells, representing podocytes and glomerular endothelial cells, respectively, were absent from the scRNA-Seq cell cluster breakdown plot from Patient C. Immunofluorescence on kidney cryosections in the 4 patients showed weaker podocin and CD31 signals in this patient, suggesting compromised function of podocytes and glomerular endothelial cells. Abnormal glomerular circulation likely resulted in podocyte dysfunction and stressed glomerular endothelial cells and podocytes would be less likely to survive enzyme (protease) treatment during cell dissociation. Hence, they would be more difficult to preserve, resulting in loss of cells with positive glomerular endothelial cell and podocyte markers on the scRNA-Seq cell cluster feature plot.

This result demonstrates the need to consider kidney histology when performing scRNA-Seq. A histology study can screen kidney samples for diseases that may reduce viability of select cell types after kidney cell dissociation and long-term storage in LN2. Similar assessments are performed in deceased donor kidneys prior to implantation; correlations with transplant outcomes are accurate when biopsies are read by expert nephropathologists[14]. We verified specific glomerular cell marker signals using immunofluorescence on kidney cryo-sections, as this was more likely to capture the native form of immunogens. Retrieving a relatively viable

kidney cell pool is critical to using cell-specific gene expression profiles from scRNA-Seq to investigate mechanisms underlying kidney disease. We conclude it is important to consider histologic screening of biopsy samples before scRNA-Seq analysis. Single nuclear RNA sequencing may avoid the requirement to assess healthy viable cells; however, mature cytosolic transcript isoforms and mitochondrial encoded transcripts will not be detected by this method. Hence, for kidney diseases resulting from mitochondrial dysfunction, such as Mitochondrial Encephalopathy, Lactic Acidosis, and Stroke-like episodes (MELAS) syndrome and recently recognized *APOL1*-associated kidney disease, scRNA-Seq may be preferable.

A limitation of this study is only four biopsies were selected for an exploratory analysis. One displayed abnormal histological findings localized to the arteriolar and microcirculatory kidney compartment, with associated tubular epithelial damage. The scRNA-Seq feature plot was consistent with our pathological finding of glomerular ischemic injury. As scRNA-Seq technology is increasingly popular, we feel the kidney community needs to be aware of potential confounders. In addition, we highlight our modified cell dissociation protocol that avoids the need to transport cryo-preserved samples to central laboratories[15] and bypasses FACS to simplify the cell processing to fit larger scale clinical biopsy-based cell-specific glomerular gene expression analyses. This approach preserves a high cell viability rate by adding a recovery stage between cell dissociation and a single-time cryo-preservation of glomerular-enriched cells in LN2, allowing future scRNA-Seq analysis to be uniformly conducted in batches with short time windows to minimize technical variation. It also provides a practical avenue for pre-implant biopsy samples in studies on cell-specific mechanisms of long-term kidney transplant outcomes.

References:

1. Sheng X, Guan Y, Ma Z *et al.* Mapping the genetic architecture of human traits to cell types in the kidney identifies mechanisms of disease and potential treatments. *Nat. Genet.* 2021; **53**: 1322–1333.
2. Abdelwahab Elhamahmi D, Chaly T, Wei G *et al.* Kidney Discard Rates in the United States During American Transplant Congress Meetings. *Transplant. Direct* 2019; **5**: e412.
3. Ma L, Shelness GS, Snipes JA *et al.* Localization of APOL1 protein and mRNA in the human kidney: nondiseased tissue, primary cells, and immortalized cell lines. *J. Am. Soc. Nephrol. JASN* 2015; **26**: 339–348.
4. Zhao X-P, Chang S-Y, Liao M-C *et al.* Hedgehog Interacting Protein Promotes Fibrosis and Apoptosis in Glomerular Endothelial Cells in Murine Diabetes. *Sci. reports* 2018; **8**: 5958.
5. Hochane M, van den Berg PR, Fan X *et al.* Single-cell transcriptomics reveals gene expression dynamics of human fetal kidney development. *PLoS Biol.* 2019; **17**: e3000152.
6. Aue A, Hinze C, Walentin K *et al.* A Grainyhead-Like 2/Ovo-Like 2 Pathway Regulates Renal Epithelial Barrier Function and Lumen Expansion. *J. Am. Soc. Nephrol. JASN* 2015; **26**: 2704–2715.
7. Mari C, Winyard P. Concise Review: Understanding the Renal Progenitor Cell Niche In Vivo to Recapitulate Nephrogenesis In Vitro. *Stem cells Transl. Med.* 2015; **4**: 1463–1471.
8. Zhang J, Pippin JW, Krofft RD *et al.* Podocyte repopulation by renal progenitor cells following glucocorticoids treatment in experimental FSGS. *Am. J. Physiol. Ren. Physiol.* 2013; **304**: F1375–F1389.
9. Seron D, Cameron JS, Haskard DO. Expression of VCAM-1 in the normal and diseased kidney. *Nephrol. Dial. transplantation: Off. Publ. Eur. Dial. Transpl. Assoc. - Eur. Ren. Assoc.* 1989; **6**: 917–922.
10. Hill PA, Main IW, Atkins RC. ICAM-1 and VCAM-1 in human renal allograft rejection. *Kidney Int.* 1995; **47**: 1383–1391.
11. Liao J, Yu Z, Chen Y *et al.* Single-cell RNA sequencing of human kidney. *Sci. data* 2020; **7**: 4.
12. He B, Chen P, Zambrano S *et al.* Single-cell RNA sequencing reveals the mesangial identity and species diversity of glomerular cell transcriptomes. *Nat. Commun.* 2021; **12**: 2141.
13. Wagner MC, Rhodes G, Wang E *et al.* Ischemic injury to kidney induces glomerular podocyte effacement and dissociation of slit diaphragm proteins Neph1 and ZO-1. *J. Biol. Chem.* 2008; **283**: 35579–35589.
14. Husain SA, King KL, Batal I *et al.* Reproducibility of Deceased Donor Kidney Procurement Biopsies. *Clin. J. Am. Soc. Nephrol. CJASN* 2020; **15**: 257–264.
15. Rao DA, Arazi A, Wofsy D *et al.* Design and application of single-cell RNA sequencing to study kidney immune cells in lupus nephritis. *Nat. Rev. Nephrol.* 2020; **16**: 238–250.

Figure 1a

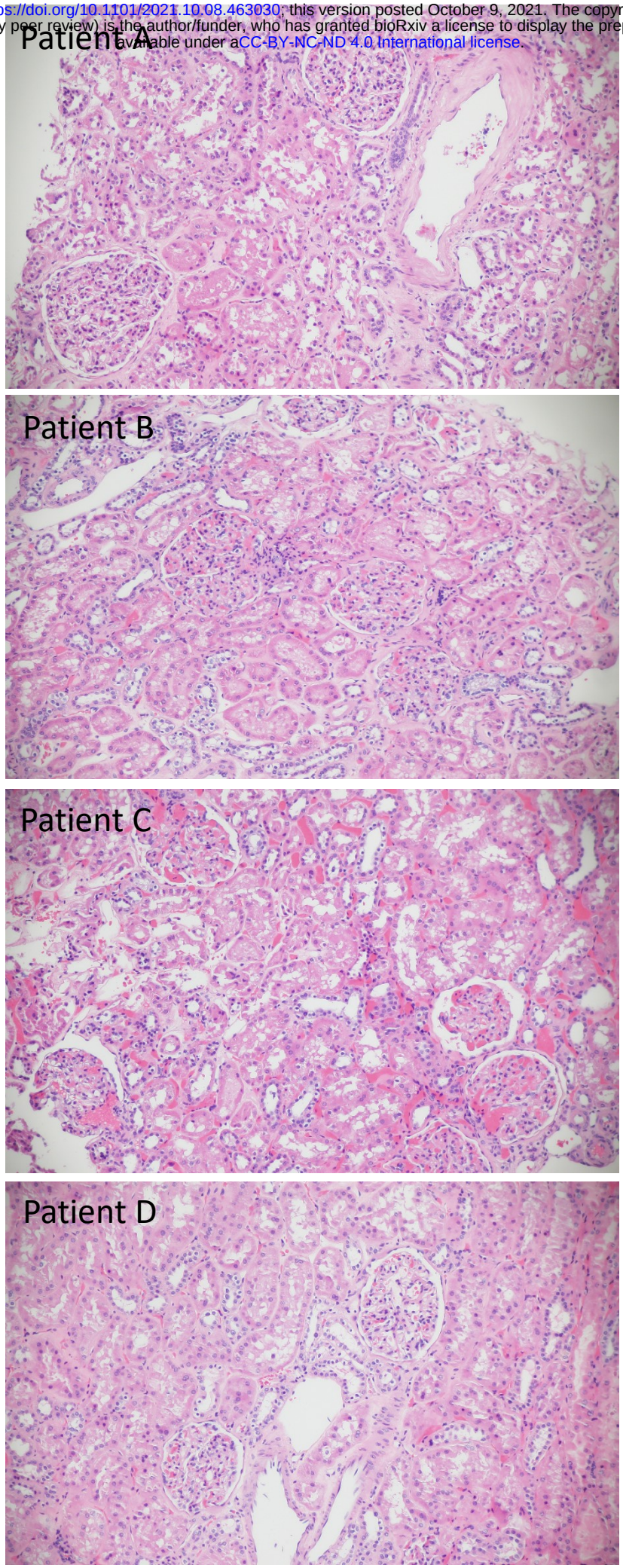

Figure 1. Hematoxylin and Eosin staining of FFPE kidney sections. Patient A, B and D had normal glomeruli and tubules. Patient C showed congested arterioles and peritubular capillaries, and acute tubular injury (All x20).

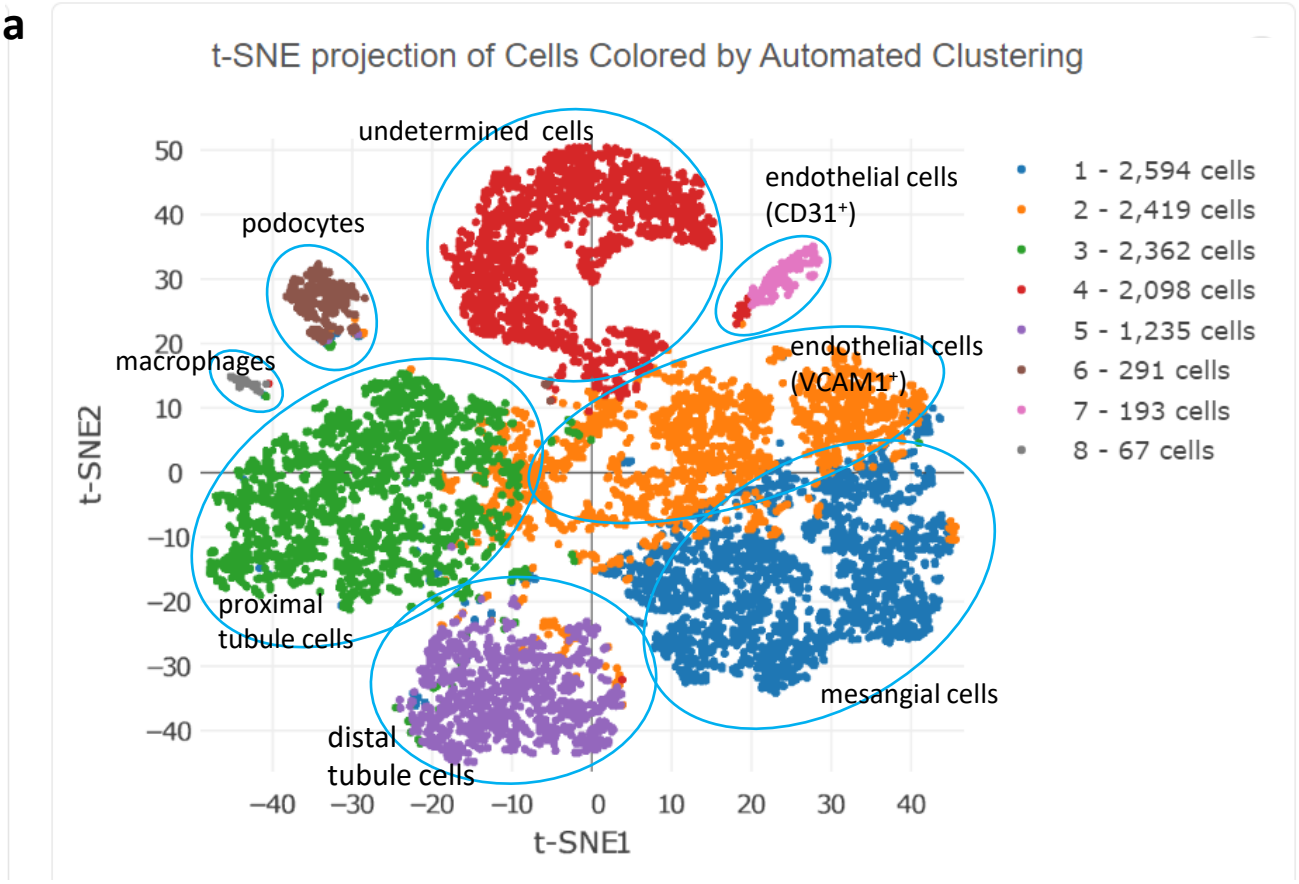

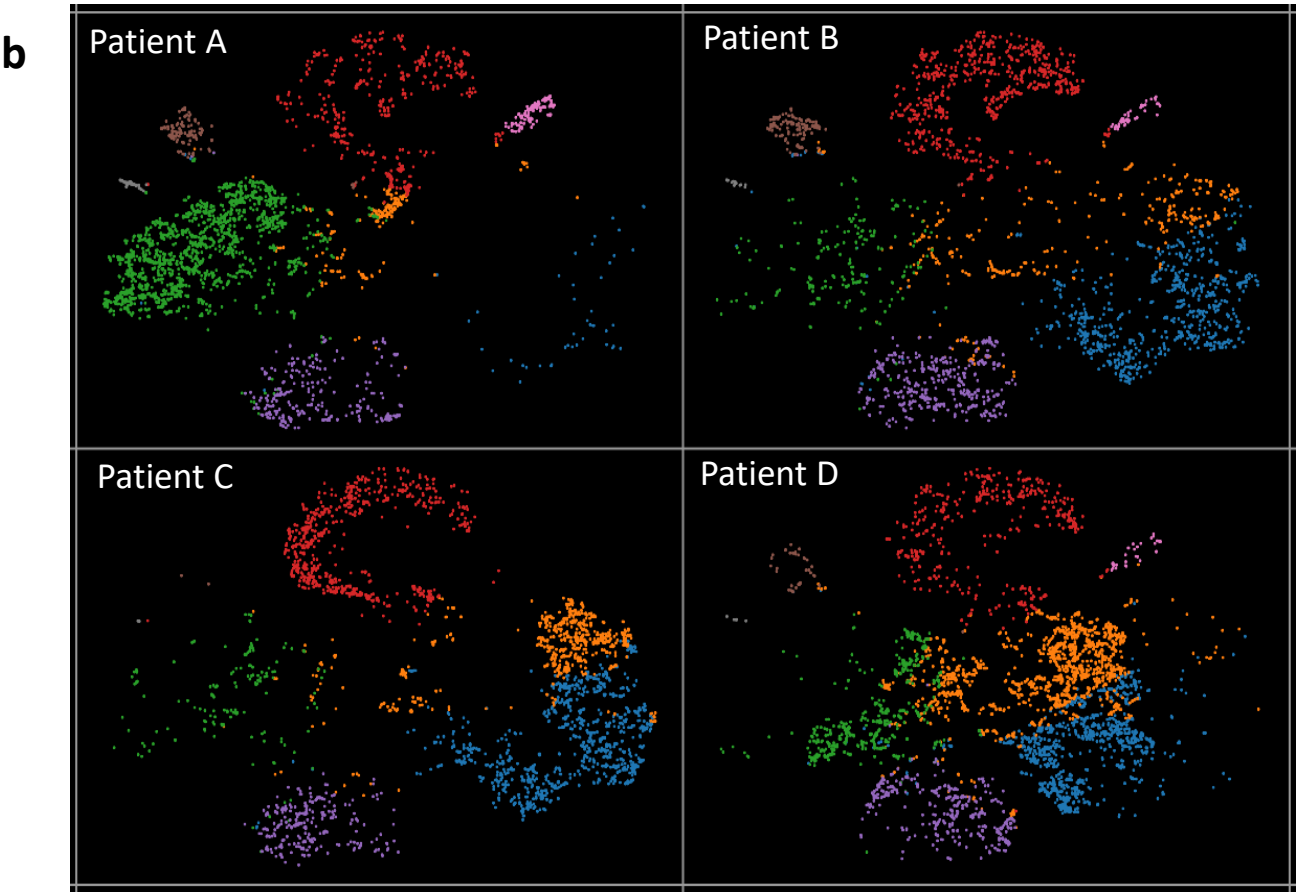

Figure 2. Feature cluster plot of enriched glomerular cells. a) Aggregation of cells from all 4 participants; b) cell clustering for individual participants.

Supplementary Table S1. Demographic data in study participants at nephrectomy

Patient	**Age** (years)	**Sex**	**BMI**[1] (kg/m^2)	**eGFR**[2] (ml/min/1.3m^2)	**Screat**[3] (mg/dL)	**Diabetes**
A	64	F	34.1	>60	0.57	yes
B	42	M	30.2	>60	0.89	no
C	49	M	29.1	>60	1.07	no
D	39	M	24.0	>60	0.93	no

[1] body mass index

[2] estimated glomerular filtration rate based on CKD-EPI Equation with race modifier

[3] serum creatinine concentration

Supplementary Table S2 . Primary antibodies used in immunofluorescence microscopy

Antibody	Vendor	Catlog #	Host species	Dilution
Podocin	Santa Cruz	sc22294	goat	1:50
CD31	BD BioSciences	550389	mouse	1:25
VCAM1	Invitrogen	14-1069-82	mouse	1:100

Supplementary Table S3. Top 5 transcripts in each cell cluster

Cluster	Transcript ID	Gene Name	Average expression	Log2 Fold Change	FDR p-value
Cluster 1 (mesangial cells)	ENSG00000164161	HHIP	1.770754501	3.346855606	5.79E-114
	ENSG00000122862	SRGN	6.013514236	2.418542557	3.90E-62
	ENSG00000122641	INHBA	2.243671826	2.456493414	3.92E-62
	ENSG00000149564	ESAM	1.376335393	2.257148582	8.32E-52
	ENSG00000154096	THY1	5.367349971	2.188619672	2.91E-51
Cluster 2 (endothelial /epithelial cells)	ENSG00000162692	VCAM1	6.244987886	2.234213085	5.69E-38
	ENSG00000123243	ITIH5	0.559389517	2.280479628	4.02E-35
	ENSG00000115414	FN1	4.393602181	1.942534372	7.69E-25
	ENSG00000128510	CPA4	1.396945406	1.804621491	1.76E-22
	ENSG00000138061	CYP1B1	1.916087407	1.652979805	1.04E-18
Cluster 3 (proximal tubule cells)	ENSG00000166825	ANPEP	2.447790385	3.444097315	4.80E-123
	ENSG00000155465	SLC7A7	0.754862593	3.436224251	2.72E-112
	ENSG00000163762	TM4SF18	0.977080569	3.365069039	2.74E-109
	ENSG00000106538	RARRES2	3.705187906	3.016146165	2.83E-95
	ENSG00000147872	PLIN2	12.46880334	2.983199759	3.85E-95
Cluster 4 (undetermined cells)	ENSG00000269028	MTRNR2L12	282.0376295	5.970255402	7.84E-135
	ENSG00000255823	MTRNR2L8	27.7000575	4.486079275	5.42E-54
	ENSG00000228253	MT-ATP8	30.39072777	4.227321278	3.36E-45
	ENSG00000198695	MT-ND6	25.78777306	4.196546371	5.79E-44
	ENSG00000212907	MT-ND4L	89.25615662	4.052794405	3.36E-40
Cluster 5 (distal tubule and collecting duct cells)	ENSG00000132698	RAB25	1.675818371	6.308897449	1.60E-299
	ENSG00000172005	MAL	5.70464003	5.966132109	2.03E-293
	ENSG00000189334	S100A14	3.867240195	5.730855672	1.67E-262
	ENSG00000137440	FGFBP1	1.659103047	6.357448663	4.71E-252
	ENSG00000184292	TACSTD2	3.53207652	5.018704904	3.17E-217
Cluster 6 (podocytes)	ENSG00000116218	NPHS2	10.94052985	9.389596611	6.23E-265
	ENSG00000011465	DCN	20.52244915	8.095615616	8.96E-261
	ENSG00000137573	SULF1	5.134592593	7.949736089	9.93E-222
	ENSG00000151490	PTPRO	4.654302536	7.862575951	7.12E-196
	ENSG00000128567	PODXL	16.34578314	6.962774549	2.40E-193
Cluster 7 (endothelial cells)	ENSG00000261371	PECAM1	18.94479545	9.756635655	8.93E-151
	ENSG00000164283	ESM1	34.04901939	9.306293451	2.86E-126
	ENSG00000176435	CLEC14A	4.356695749	10.45237589	1.96E-104
	ENSG00000162618	ADGRL4	9.654559221	8.989368172	2.13E-102
	ENSG00000142748	FCN3	18.26168985	10.38980679	3.40E-99
Cluster 8 (macrophages)	ENSG00000173372	C1QA	55.0570153	11.7952818	5.00E-157
	ENSG00000173369	C1QB	66.63062028	11.79327393	3.26E-154
	ENSG00000011600	TYROBP	20.66576701	11.79985155	3.58E-147
	ENSG00000159189	C1QC	25.43479017	11.79249695	1.60E-139
	ENSG00000158869	FCER1G	22.2554414	11.28423297	3.09E-133

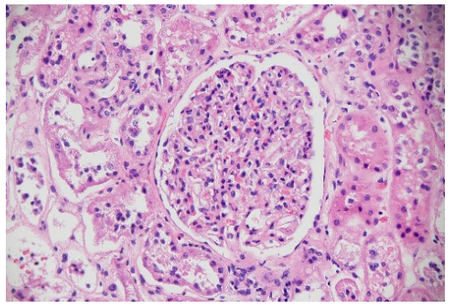

Histological assessment

Kidney tissue sections with collagenase

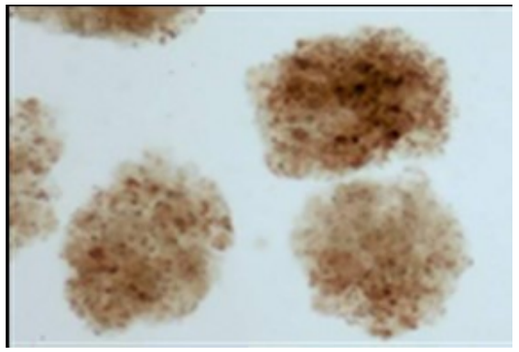

Glomeruli-enriched kidney tissue collected by a cell strainer

Cell dissociation

Cell Recovery

Resuspend cells and storage in LN2

Illumina NextSeq500

scRNA-Seq

FFPE sections

Cold transport on ice

Kidney Biopsy: Study Start

Cryo-sections for immunofluorescence

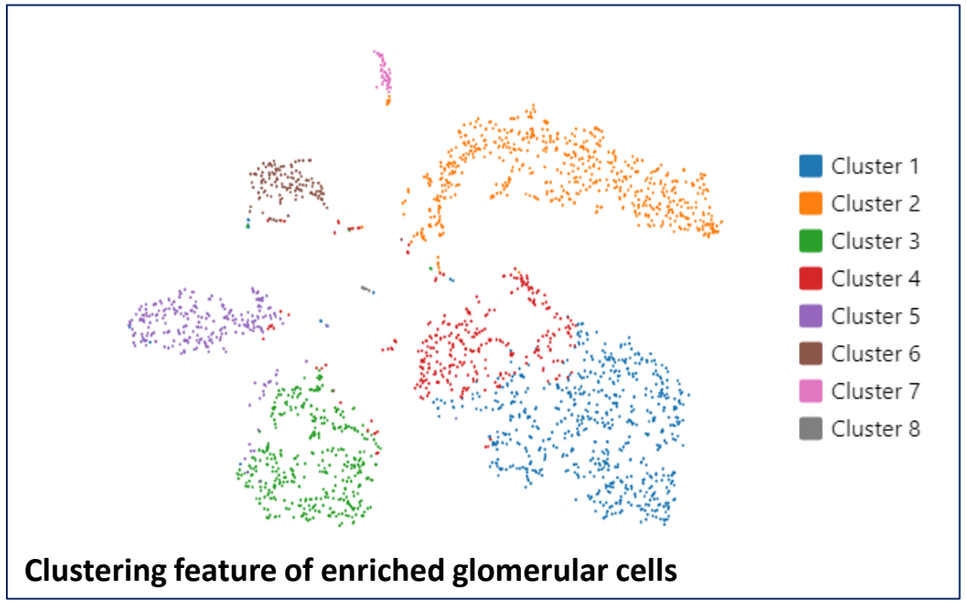

Clustering feature of enriched glomerular cells

Supplementary Figure S1. Study design, representative data, and technical outline

Note: The photos in this diagram are actual imaging and analytical data from one representative participant.

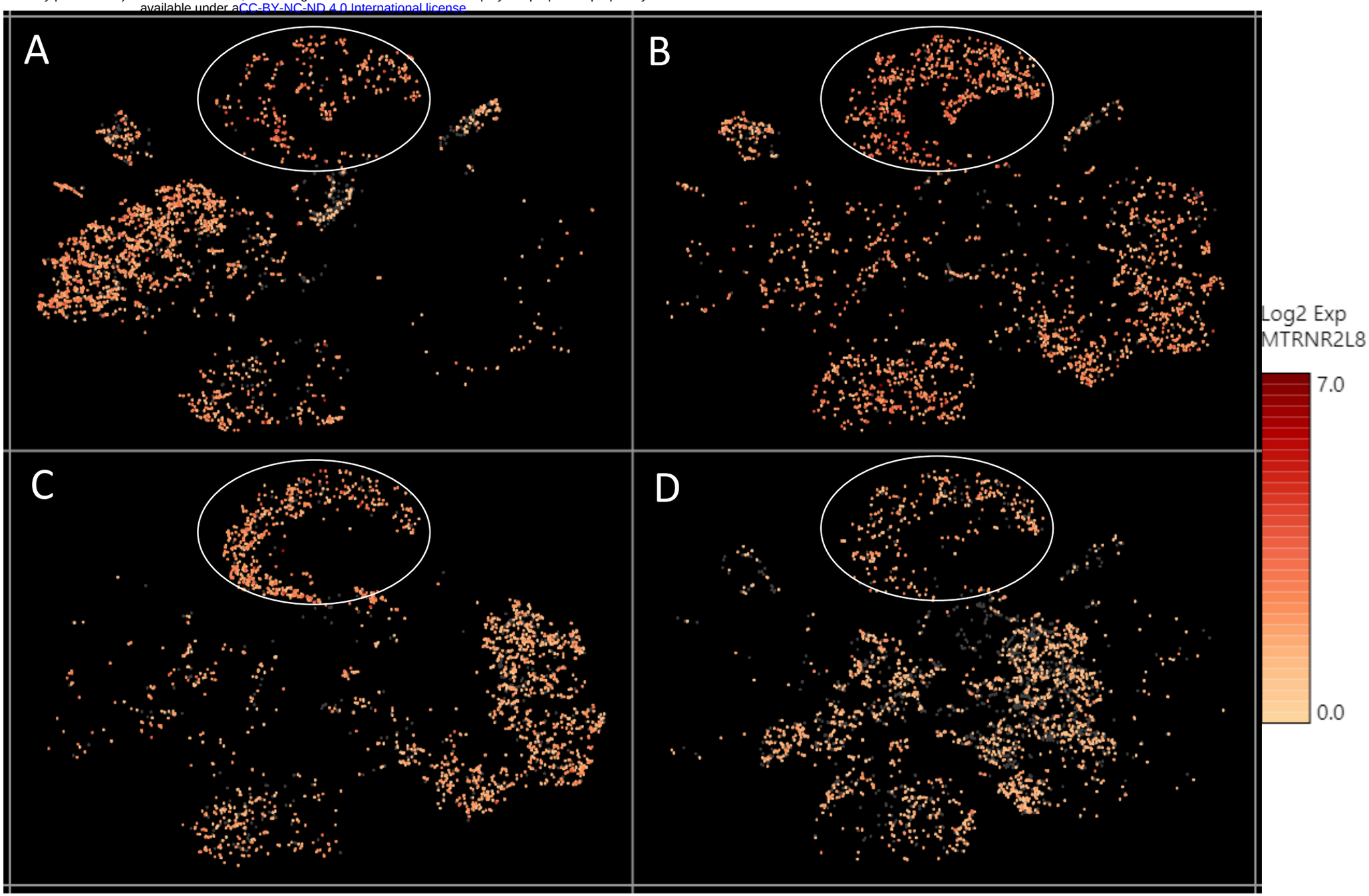

Supplementary Figure S2. The relative expression level of a mitochondrial encoded transcript *MTRNR2L8* across different cell clusters. *MTRNR2L8* levels were higher in the “undetermined“ cells (circled), compared to other cell types

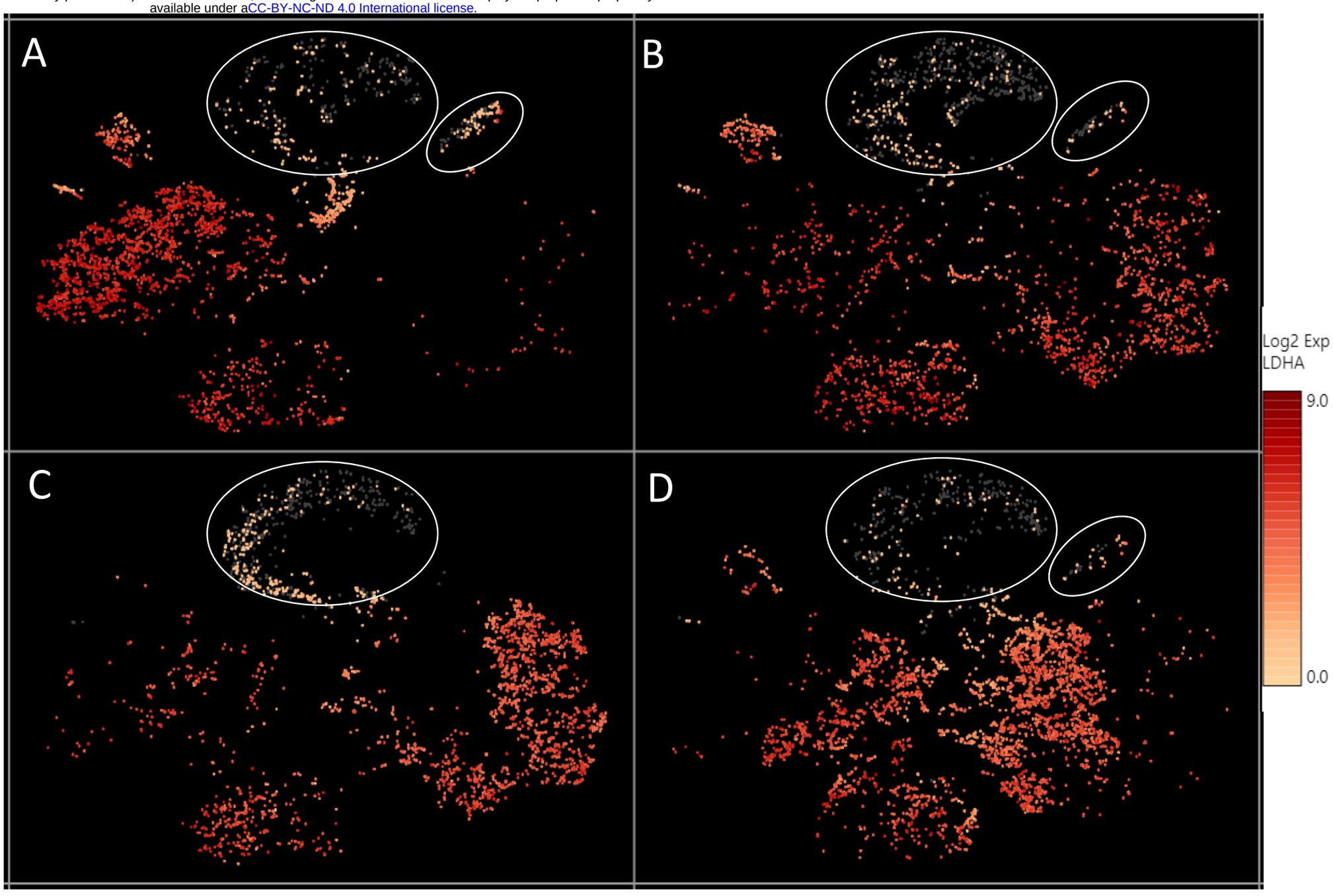

Supplementary Figure S3. The relative expression level of the *LDHA* transcript across different cell clusters. *LDHA* levels were lower in the “undetermined“ and podocyte cell clusters (circled), compared to other cell types

Supplementary Figure S4

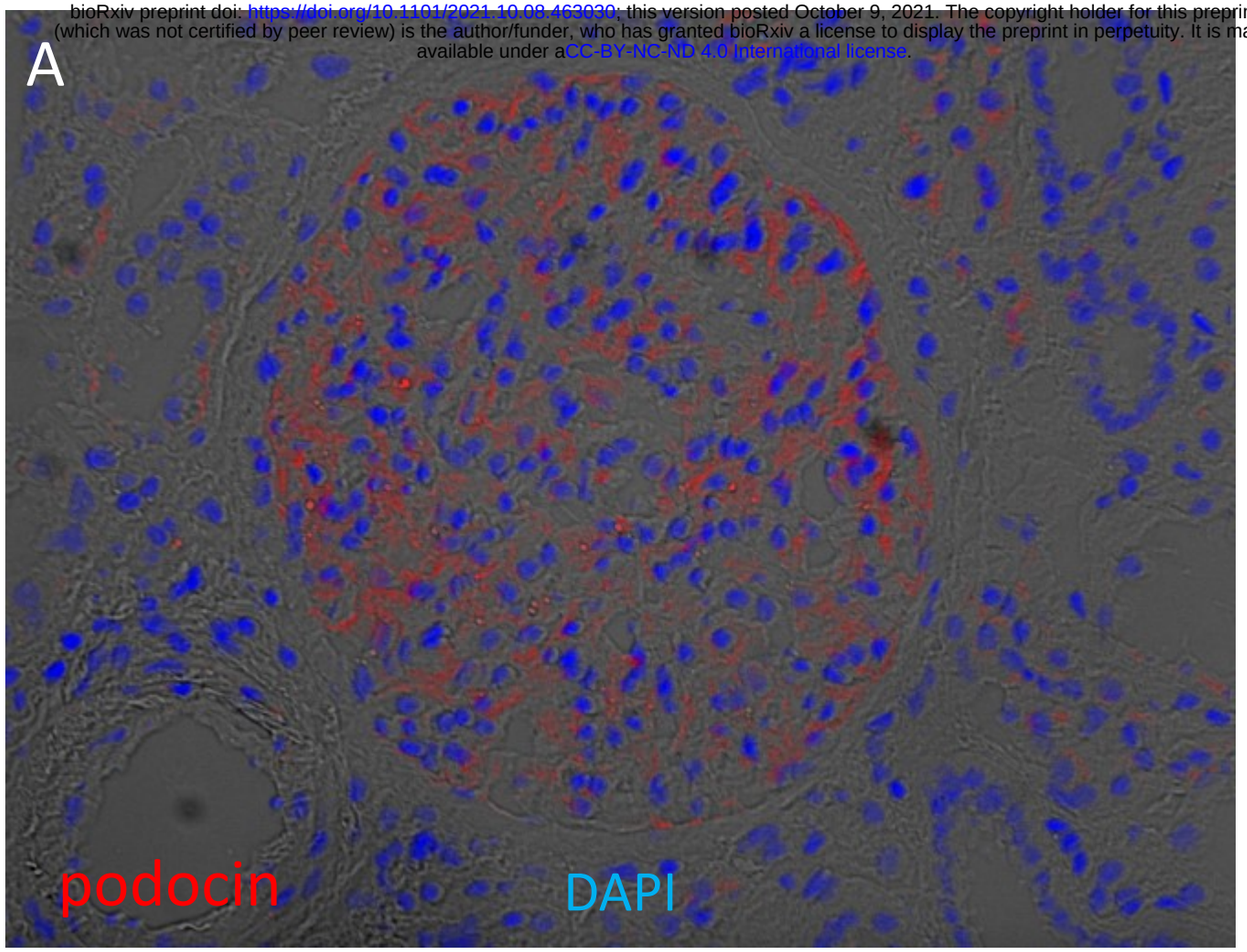

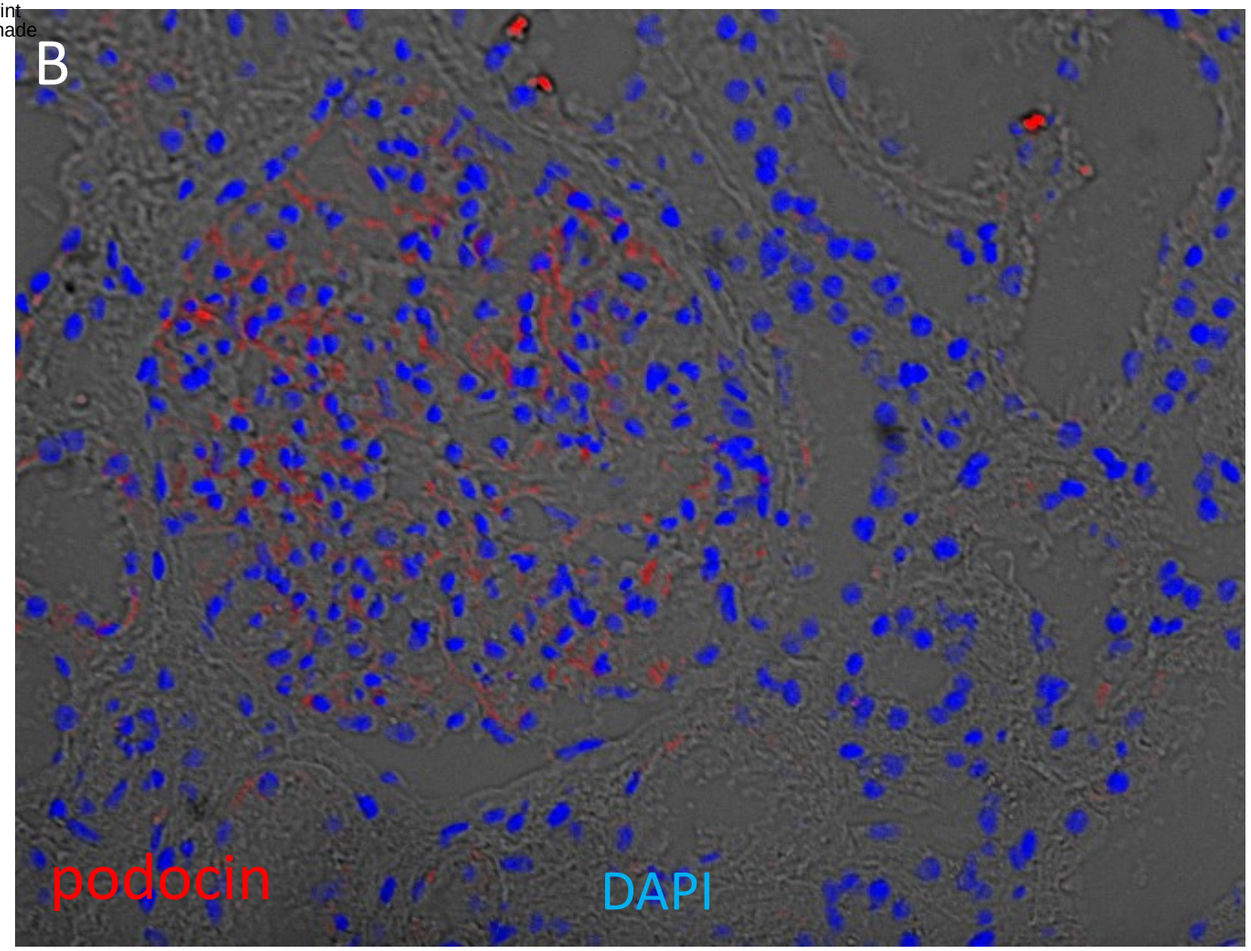

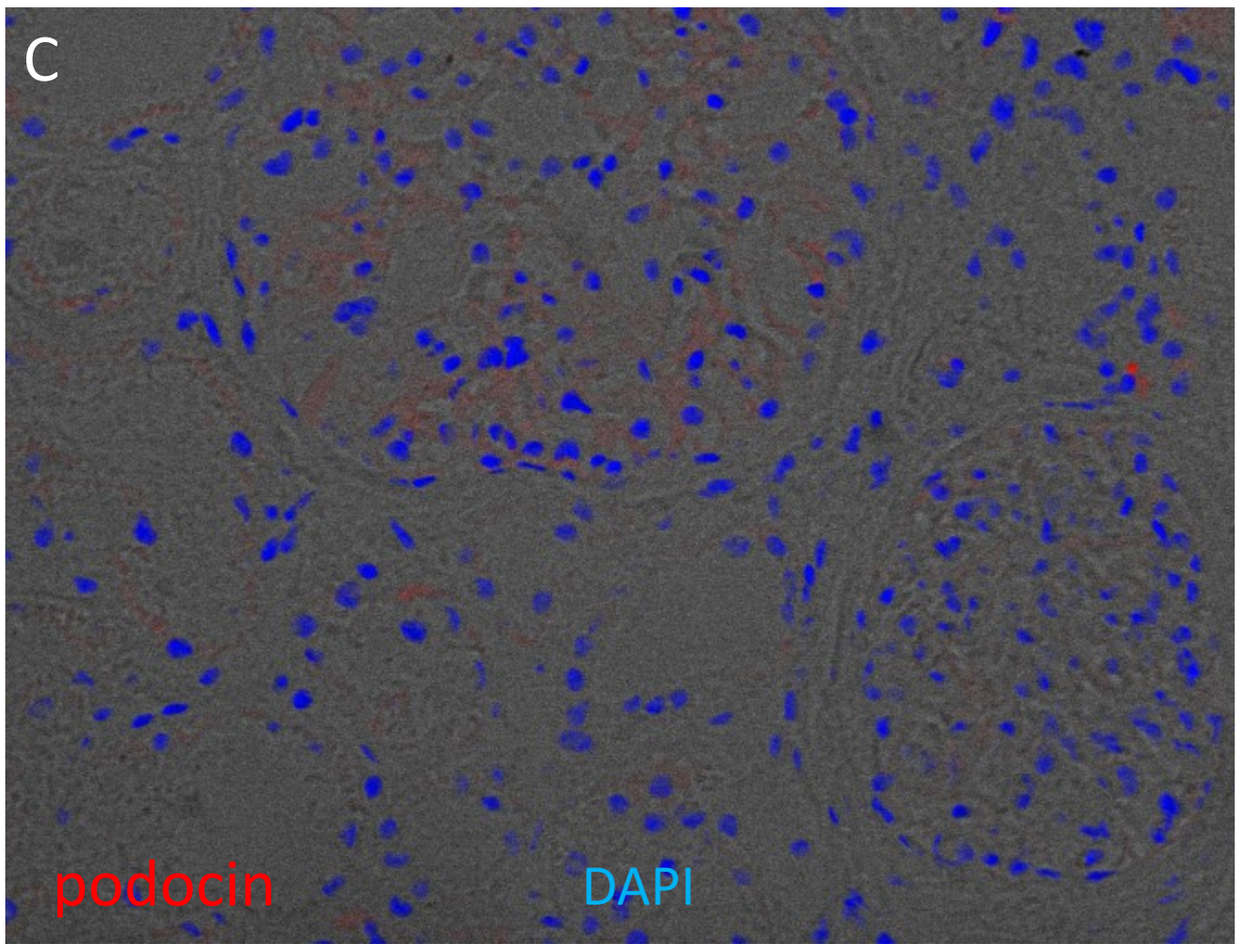

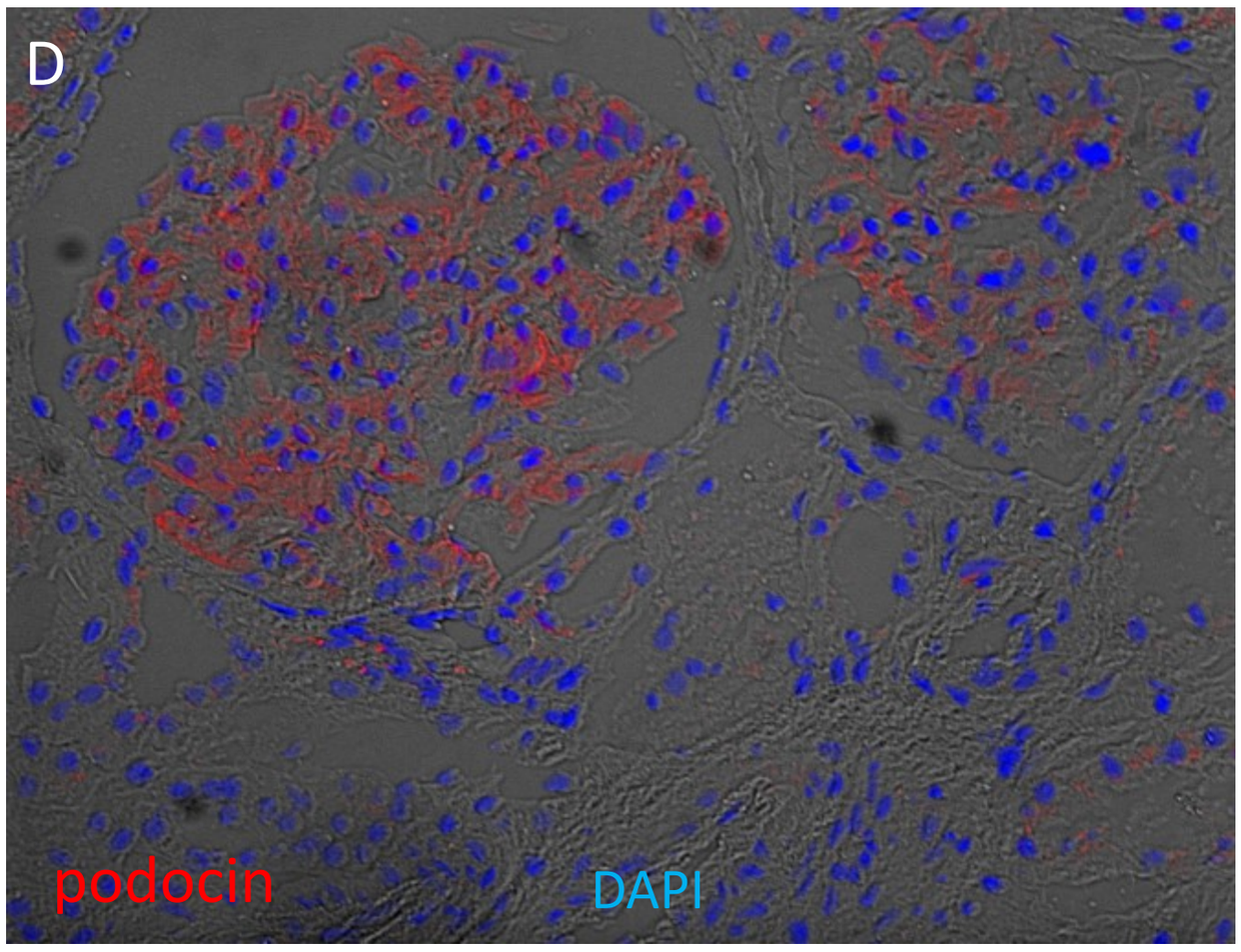

Supplementary Figure S4. Glomerular enrichment of podocin on kidney cryosections. Immunofluorescence of podocin was performed on four kidney cryosections from European Americans without known kidney disease. Cryosections were stained for podocin (red) and counterstained with 4’,6-diamidino-2-phenylindole (DAPI) (blue) overlapped with bright field. Podocin signals are enriched in glomeruli, with weaker expression in participant C.

Supplementary Figure S5

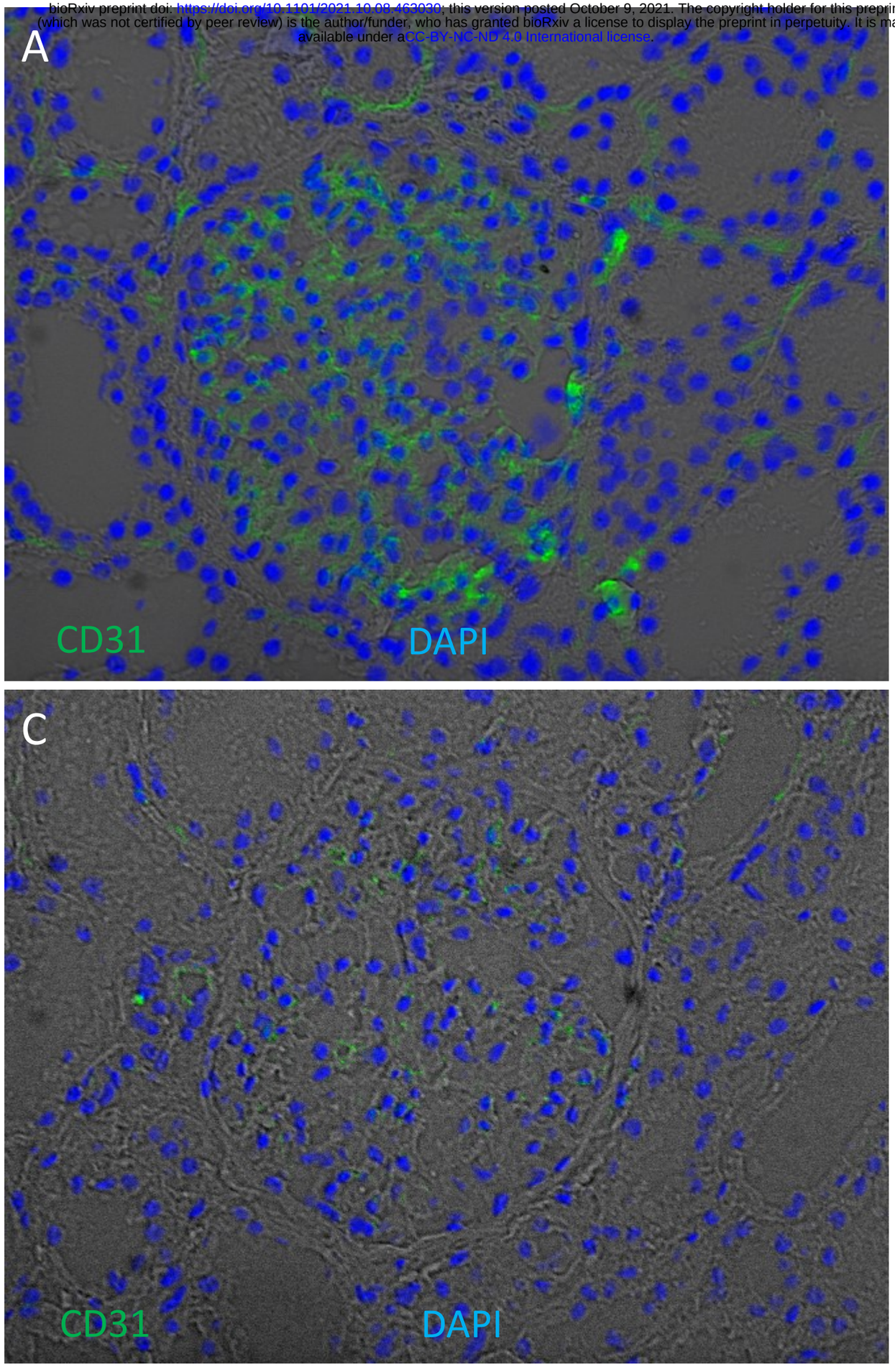

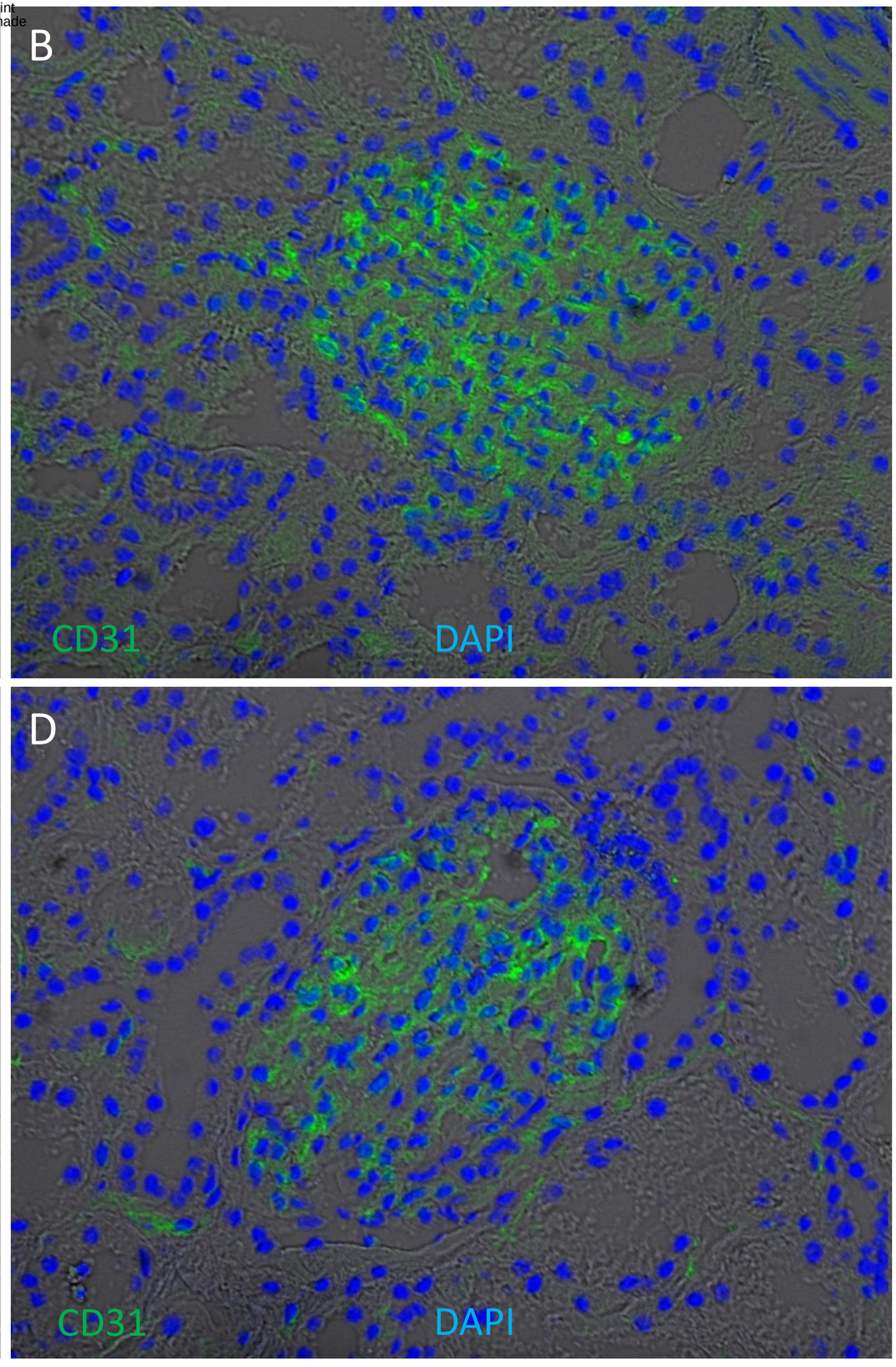

Supplementary Figure S5. Glomerular enrichment of CD31 on kidney cryosections. Immunofluorescence of CD31 was performed on four kidney cryosections from European Americans without known kidney disease. Cryosections were stained for CD31 (green) and counterstained with 4’,6-diamidino-2-phenylindole (DAPI) (blue) overlapped with bright field. CD31 signals are enriched in glomeruli, with weaker expression in participant patient C.

Supplementary Figure S6

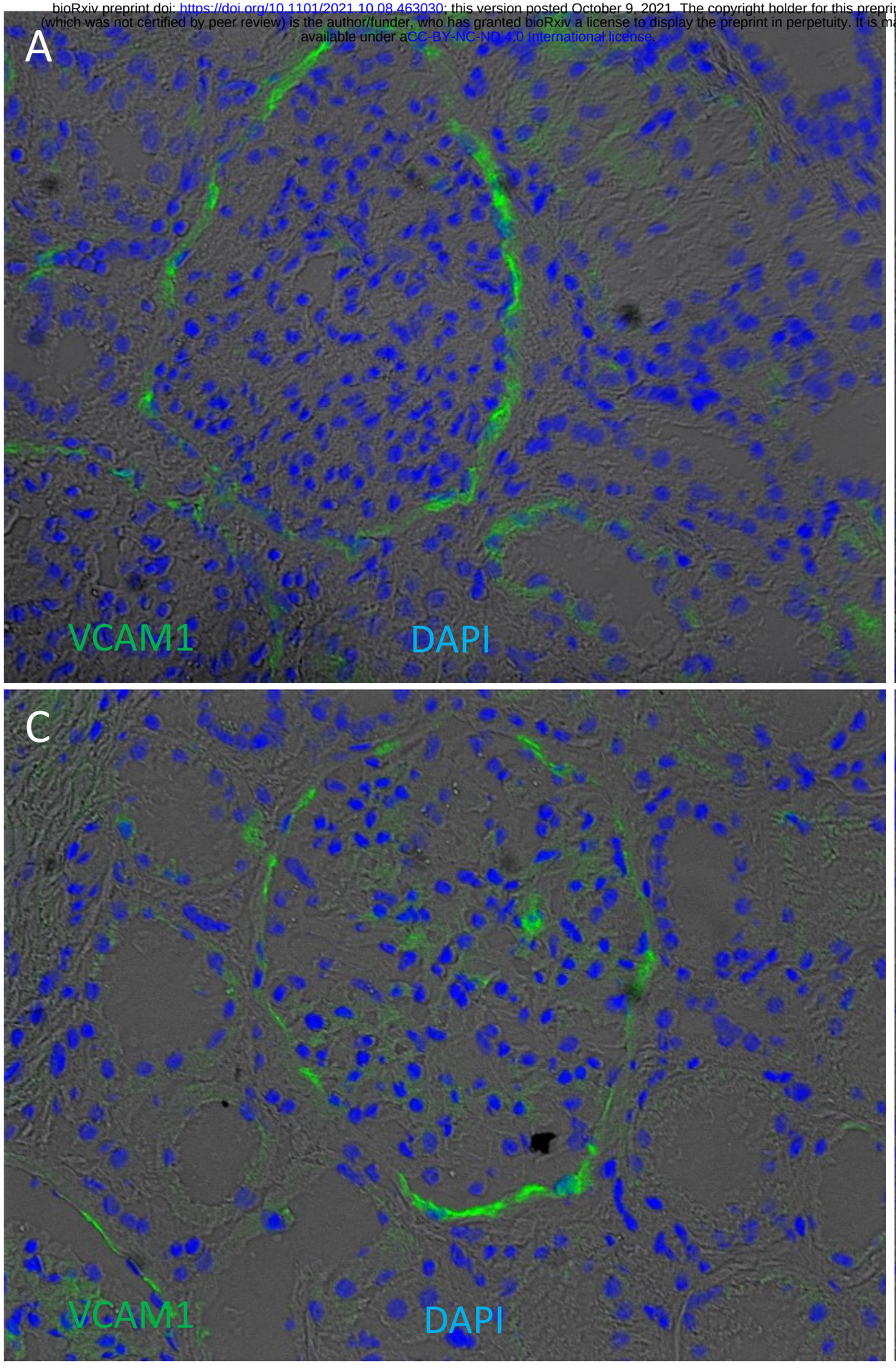

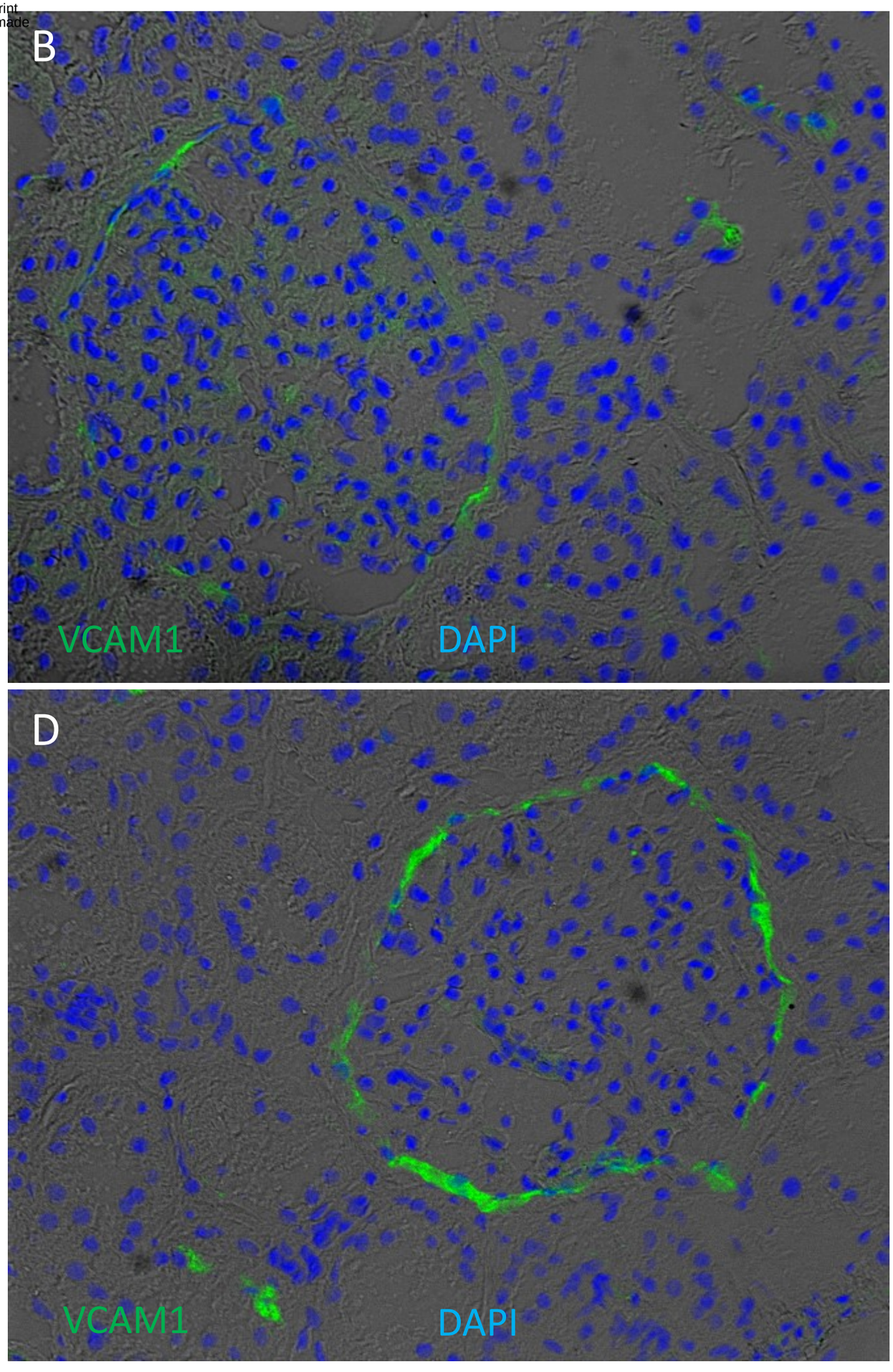

Supplementary Figure S6. Presence of VCAM1 on kidney cryo-sections. Immunofluorescence of VCAM1 was performed on four adult Caucasian kidney cryosections without known native kidney disease. Kidney cryosections were stained for VCAM1 (green) and counterstained with 4’,6-diamidino-2-phenylindole (DAPI) (blue) overlapped with bright field. VCAM1 appeared to enriched in cells lining Bowmen capsule and peritubular endothelial cells.